Sains Malaysiana 49(11)(2020): 2821-2832
http://dx.doi.org/10.17576/jsm-2020-4911-21

First-Principles Study of Structural, Electronic and Thermoelectric Properties of Ni-Doped Bi_2Se_3

(Kajian Prinsip Pertama tentang Sifat Struktur, Elektronik dan Termoelektrik bagi Bi_2Se_3 Ni-Terdop)

MUHAMMAD ZAMIR MOHYEDIN, MOHAMAD FARIZ MOHAMAD TAIB*, AFIQ RADZWAN, MASNAWI MUSTAFFA, AMIRUDDIN SHAARI, BAKHTIAR UL-HAQ, OSKAR HASDINOR HASSAN & MUHD ZU AZHAN YAHYA

ABSTRACT

Direct conversion of waste heat to electrical energy could address present energy challenges. Bi_2Se_3 is one of few thermoelectric materials known to operate at room temperature. Comprehensive analysis using density functional theory was conducted to explore the effect of nickel doping on structural, electronic, and thermoelectric properties of Bi_2Se_3. Local density approximation (LDA) was used with an addition of spin-orbit coupling (SOC) and van der Waals *interaction scheme consideration. Analysis of the effect of SOC was elaborated. It was found that nickel has changed the crystal structure of Bi_2Se_3. Nickel has also changed band structure and density of state that alter the thermoelectric performance. The decreased band gap has decreased the thermopower. However, it gives advantages to the improvement of electrical conductivity. Higher electrical conductivity has risen thermal conductivity. Despite the decreased thermopower and increased thermal conductivity, the higher electrical conductivity has improved the overall thermoelectric performance of Bi_2Se_3 when nickel is introduced.*

Keywords: Density functional theory; electrical conductivity; electronic properties; spin-orbit coupling; thermoelectricity

ABSTRAK

Penukaran sisa haba kepada tenaga elektrik dapat menangani cabaran tenaga yang ada pada masa ini. Bi_2Se_3 adalah salah satu daripada beberapa bahan termoelektrik yang diketahui mampu beroperasi pada suhu bilik. Analisis komprehensif menggunakan teori ketumpatan berfungsi telah dijalankan untuk meneroka kesan pendopan nikel pada sifat struktur, elektronik dan termoelektrik Bi_2Se_3. Penghampiran ketumpatan setempat (PKS) digunakan dengan mempertimbangkan penambahan gandingan spin-petala (GSP) dan skema interaksi van der Waals. *Analisis kesan GSP dijelaskan. Didapati bahawa nikel telah mengubah struktur kristal Bi_2Se_3. Nikel juga telah menukar struktur jalur dan ketumpatan keadaan yang mengubah prestasi termoelektrik. Penurunan jurang jalur telah menurunkan termokuasa. Walau bagaimanapun, ia memberi kelebihan kepada peningkatan kekonduksian elektrik. Kekonduksian elektrik yang tinggi telah meningkatkan kekonduksian terma. Walaupun termokuasa menurun dan kekonduksian terma meningkat, kekonduksian elektrik yang lebih tinggi telah meningkatkan prestasi termoelektrik keseluruhan Bi_2Se_3 apabila nikel diperkenalkan.*

Kata kunci: Gandingan spin-petala; kekonduksian elektrik; sifat elektronik; teori ketumpatan berfungsi; termoelektrik

INTRODUCTION

Thermoelectric materials have received wide attention due to its ability to convert waste heat to electricity especially some of the materials that can effectively operating at room temperature (Bashir et al. 2018; Hasan et al. 2018). It could also potentially become one of the solutions for energy and environmental crisis like global warming (Saeed et al. 2014b). Its high-performance provides a great contribution to the society for its application in thermoelectric refrigeration (Mishra et al. 1997), radiation detector (Augustine et al. 2003) and environmental protector (Saeed et al. 2014b). The performance of thermoelectric material can be described by a dimensionless figure of merit (ZT):

$$ZT = \frac{S^2 \sigma T}{\kappa}$$

where S is the Seebeck Effect or thermopower; σ is electrical conductivity; T is the temperature; and κ

is thermal conductivity. From the equation, a good thermoelectric material should possess high electrical conductivity and lower thermal conductivity. Bismuth selenide (Bi_2Se_3) is one of the excellent candidates for thermoelectric application due to the ability to operate at room temperature (Min et al. 2015), as compared to other thermoelectric materials that operate at elevated temperature (Chang et al. 2016; Tan et al. 2015, 2014). Additionally, Bi_2Se_3 is also a topological insulator, a new quantum state of matter that gives the thermoelectric material unique properties that could conduct electricity on its surface or edge, but still having insulating behaviour in the bulk (Xu et al. 2017). Among the topological insulators, Bi_2Se_3 is one of the most extensively studied because of its simplicity surface state which made up of a single Dirac cone at the Γ point (Aguilera et al. 2013). This discovery could make this material a promising candidate to be applied such as on spintronic devices (Mirhosseini & Henk 2012), topological quantum computing (Lin et al. 2013), and magnetic memories (Chis et al. 2012).

Despite the advantages of Bi_2Se_3 that can operate at room temperature, the thermoelectric performance at its pure form in room temperature is very low which has figure of merit around 0.01 - 0.05 (Kulsi et al. 2017; Min et al. 2015, 2013). Therefore, many attempts have been done to increase the thermoelectric performance of Bi_2Se_3. Many experimental methods have been conducted that show different performance which indicates that method gives influence on the performance. Scalable exfoliation strategy has improved Bi_2Se_3 performance up to 0.11 figure of merit (Sun et al. 2012). Pulsed magnetic field method increased the Bi_2Se_3 performance to 0.14 (Kulbachinskii et al. 2012). In addition, different types of nano-structure also influence the performance of Bi_2Se_3 such as nanoplates structure that gives Bi_2Se_3 figure of merit 0.14 (Ali et al. 2014). There are also many efforts to enhance the performance by using a doping method such as reported by Hor et al. (2009) that using calcium as a dopant and get figure of merit 0.07. Doped by using Cu and Fe increased the performance to 0.10 (Dun et al. 2015; Saeed et al. 2014b). There was also an effort to increase the power factor by doping with TI and Cr (Cermak et al. 2018; Janíček et al. 2009).

This work will use another transition metal, Ni to increase the thermoelectric performance of Bi_2Se_3. Besides that, we intended to investigate the underlying mechanism of the enhanced thermoelectric performance by conducting a comprehensive analysis of the effect of Ni on the structural and electronic properties of Bi_2Se_3. We expected the role of Ni will reduce bond length and band gap that indicates increased electron participation.

COMPUTATIONAL DETAILS

The calculation was performed using the rhombohedral structure of Bi_2Se_3 with the space group . The initial structure of Bi_2Se_3 was taken from the experimental study by Nakajima (1963). Structural optimization was performed by using CASTEP within pseudo-potential with cut-off energy 400 eV and k-points 3×3×1 after convergence test was done. The optimization was done within local density approximation (LDA) exchange-correlation and Perdew-Burke-Ernzerhof revised for solids (PBESol) approximation (Perdew & Zunger 1981). Van der Waals interaction scheme was considered. The structural properties that consist of bond length, lattice parameter and bond order were calculated by optimizing the structure.

Electronic properties were performed using WIEN2K (Blaha et al. 2001) computer code within full-potential linearized-augmented plane-wave (FP-LAPW) and exchange-correlation of LDA (Perdew & Zunger 1981). The electronic properties calculation which are band structure, the density of states (DOS) and charge density were performed with the inclusion of spin-orbit coupling (SOC) to analyse its effect on the material (Richards et al. 1981).

The calculation of thermoelectric properties was performed by Boltzmann Transport Properties (BoltzTraP) that implemented within the package of WIEN2K (Madsen & Singh 2006). The thermopower, electrical conductivity, thermal conductivity, and figure of merit (ZT) were evaluated over temperature from 300 to 500 K. The calculation was performed under the plane-wave cut off of 8.0 and k-points mesh of 1000.

STRUCTURAL OPTIMIZATION

In this work, the structural optimization was performed to stabilize the geometric cells and the structure of Bi_2Se_3 and Ni-doped Bi_2Se_3. Structural properties which are bond length, lattice parameter, and bond order were calculated. Figure 1 shows an optimization structure of Bi_2Se_3.

Bi_2Se_3 is a rhombohedral structure that consists of five-atom layers arranged along z-direction by the repeated atom sequences of Se(1) – Bi – Se(2) – Bi – Se(1). These layers are known as quintuple layer. The bonding within the quintuple layer is strong but much weaker between two quintuple layers that are bonded by van der Waals interaction. Table 1 shows the structural properties of Bi_2Se_3 and Ni-doped Bi_2Se_3.

Our result averagely consistent with experimental studies. Within LDA calculation, lattice *a* averagely overestimate only by 0.05%, while lattice *c* averagely

underestimates by 5.14%. Within GGA-PBESol calculation, lattice a averagely underestimate by 0.19%, while lattice *c* averagely underestimates by 0.57%. LDA calculation has more consistent value on lattice *a*, while GGA-PBESol has more consistent value with lattice *c* when compared with experimental studies. Since the gap of consistency between LDA and PBESol is not having a large difference, LDA was chosen to optimize the structure of Ni-doped Bi_2Se_3 and to calculate the electronic and thermoelectric properties of undoped and doped Bi_2Se_3. LDA was chosen to save cost, time and energy since LDA has less parameter to calculate when compared with PBESol. Doping with Ni has changed the lattice parameter of Bi_2Se_3 with *a* and *b* decreasing by 2.44%, and *c* decreasing by 10.28%. Nickel has made the whole structure of Bi_2Se_3 smaller by 14.31% from volume 404.269 $Å^3$ to 346.399 $Å^3$.

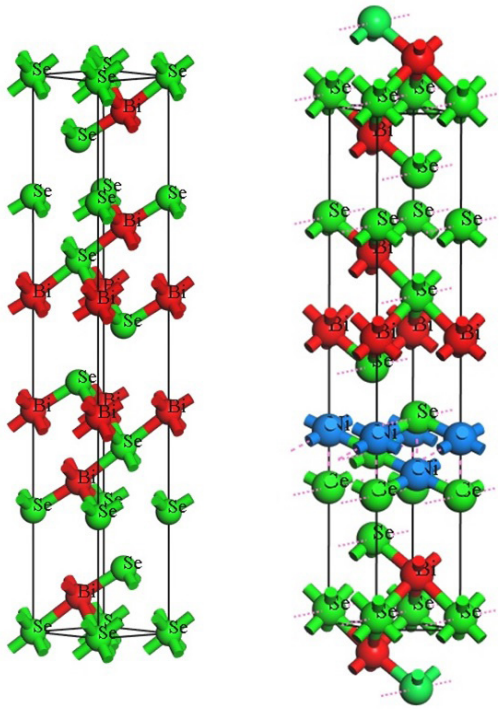

FIGURE 1. Optimized structure of Bi_2Se_3 and Ni-doped Bi_2Se_3

TABLE 1. Structural properties of Bi_2Se_3 and Ni-doped Bi_2Se_3

Method	Reference	*a*(Å)	*b*(Å)	*c*(Å)
LDA	This work (Pure)	4.147	4.147	27.221
GGA-PBESol	This work (Pure)	4.137	4.137	28.493
LDA	This work (Ni-doped)	3.993	3.993	24.963
X-ray diffraction	Experimental (Urkude et al. 2018)	4.145	4.145	28.652
X-ray diffraction	Experimental (Boledzyuk et al. 2015)	4.147	4.147	28.681
X-ray diffraction	Experimental (Nakajima 1963)	4.143	4.143	28.636

The strength of the bond can be measured through the bond length for each atomic bonding in the structure. The bond length of Bi_2Se_3 and Ni-doped Bi_2Se_3 are tabulated in Tables 2 and 3, respectively.

TABLE 2. Bond length of Bi_2Se_3

Bond	This work (Å)	Experimental (Å) (Hagmann et al. 2017)	Experimental (Å) (Lind et al. 2005)
Se (1) – Bi	2.83	2.97	2.83
Se (2) – Bi	3.04	3.04	3.04
Van der Waals Distance	3.34	3.27	3.27

The van der Waals length is 3.34 Å, which is the longest length shows the weakest bonding in the structure of Bi_2Se_3. The weak van der Waals bonding between adjacent quintuple layer has caused Bi_2Se_3 having topological surface states. The bond of Se(1) – Bi shows the shortest bond which has a length of 2.83 Å. Se (1) – Bi is the strongest bond in the structure which is located within the quintuple layer. Besides the contribution to the electron conductivity, the short bond length also contributes to the thermal conductivity due to its short-range potential. However, the significance of van der Waals in the structure is it can reduce phonon transmission throughout the material, thus, reduces thermal conductivity as reported by Park et al. (2015). The calculated bond lengths are relatively consistent with the experimental works. Se (1) – Bi underestimated by 4.95% and van der Waals length overestimated by 2.10%. The bond of Se (2) – Bi remains the same with the experimental works (Hagmann et al. 2017; Lind et al. 2005).

Nickel (Ni) atoms were doped at the van der Waals connecting atoms by substituting two atoms of Bi-lattice as shown in Figure 1. It shows the optimization structure of Ni-doped Bi_2Se_3. The presence of Ni atoms caused the bond length of Se (1) – Bi and Se (2) – Bi decreased. The van der Waals distance remains the same. The bond length of Ni-doped Bi_2Se_3 is tabulated in Table 3.

TABLE 3. Bond length of Ni-doped Bi_2Se_3

Bond	Ni-doped (Å)	Pure (Å)
Se (1) – Bi	2.82	2.83
Se (2) – Bi	3.02	3.04
Se (1) – Ni	2.44	-
Se (2) – Ni	2.51	-
Van der Waals Distance	3.34	3.34

Table 3 shows that Se (1) – Ni is the strongest bond in the structure of Ni-doped Bi_2Se_3 due to its shortest bond length. Se (1) – Bi bond has decreased by 0.35% and Se (2) – Bi bond has decreased by 0.66%. A new bond has formed within the structure which is Se (1) – Ni bond and Se (2) – Ni. Decreased bond length has increased electron participation, thus increasing the electrical conductivity. Due to the unchanged distance of van der Waals interaction, the reduction of phonons transmission remained the same. However, due to the decreased bond length, the thermal conductivity would be increased.

The bond order is calculated to analyse the stability of the bond. The results of the calculated bond order of Bi_2Se_3 and Ni-doped Bi_2Se_3 are tabulated in Table 4.

TABLE 4. Bond order of Bi_2Se_3 and Ni-doped Bi_2Se_3

Bi_2Se_3		
Bond	Bond order	
Se (1) – Bi	1.000	0.570
Se (2) – Bi	1.000	1.000
Ni-doped Bi_2Se_3		
Bond	Bond order	
Se (1) – Ni	1.000	0.760
Se (2) – Ni	1.000	0.760
Se (1) – Bi	1.000	0.485
Se (2) – Bi	1.000	1.000

Table 4 shows the bond order for each bond length of Bi_2Se_3. Se (1) – Bi have two bond orders which are 1.000 and 0.570 that indicates a mix of ionic-covalent type of bonding. Bond order of 1.000 indicates a single covalent bond, while 0.570 indicates ionic bond. Se (2) – Bi has a bond order of 1.000 that indicates a single covalent bond. 1.000 is the maximum bond order and the strongest bond of Bi_2Se_3 structure.

Nickel has made a significant change to the bond order of Bi_2Se_3. Most of the bond length has a mixed covalent-ionic type of bonding except for Se (2) – Bi. Bond Se (1) – Bi has decreased its ionic bonding by 14.91% which shows that nickel has weakened the bond. Bond of Se (2) – Bi remained as a single covalent bond. The new formed of the bond which are Se (1) – Ni and Se (2) – Ni have mix covalent-ionic type of bonding. Introducing nickel to the Bi-lattice, the ionic bonding has increased by 33.33% when compared between Se (1) – Ni and Se (1) – Bi. For Se (2) – X (X=Bi, Ni), the bond has changed from covalent bond to the mixed covalent-ionic bond.

ELECTRONIC PROPERTIES

The band structure and density of states (DOS) were calculated by using LDA as the exchange-correlation with cut-off energy 8.0 and k-points 1000. The results were compared with the other works on both experimental and theoretical studies. The band gap of Bi_2Se_3 with the inclusion of SOC is 0.23 eV while without SOC is 0.01 eV as shown in Figure 2.

The band gap between without and with the inclusion of SOC shows a huge difference up to 82.35%. The SOC band gap is consistent with a small difference of 4.26% with experimental work by Martinez et al. (2017) (0.23 eV). However, the band gap underestimates with other works by difference around 18 - 31% (Han et al. 2014; Lawal & Shaari 2017; Valla et al. 2012; Wang & Zhang 2012). On the other hand, the band gap without SOC shows inconsistency between each other (Lawal & Shaari 2017; Wang & Zhang 2012,). This proved that

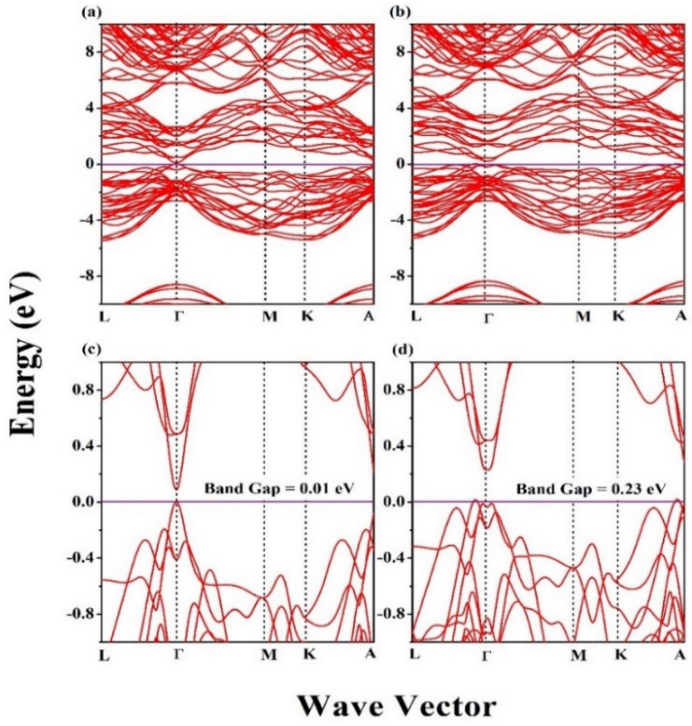

FIGURE 2. a) Band structure of Bi_2Se_3 without SOC at energy range from 10 eV to -10 eV b) Band structure of Bi_2Se_3 with SOC at energy range from -10 eV to 10 eV c) Band structure of Bi_2Se_3 without SOC at energy range from 1.0 eV to -1.0 eV d) Band structure of Bi_2Se_3 with SOC at energy range from -1.0 eV to 1.0 eV

SOC inclusion is necessary to calculate Bi_2Se_3, hence to manifest its true nature. Other theoretical works such as by Lawal and Shaari (2017) and Wang and Zhang (2012) show the same behaviour regarding this. Without the inclusion of SOC, Bi_2Se_3 could not manifest the band structure correctly compared to the inclusion of SOC.

Anti-crossing feature occurred around as a result of the effect of SOC on the band structure. This feature yields an inversion between conduction and valence band. As we can observe in Figure 2, with the inclusion of SOC the band structure formed a multi-valley band at maximum valence band instead of single-valley that shown by band structure without the inclusion of SOC. This inversion is known as spin-orbit splitting whereby the SOC splits the bands. The splitting energy occurs due to the Dresselhaus effect from the applied SOC. Without SOC, a gapless band structure would occur. SOC breaks the gapless band structure that resulting the Dresselhaus effect (Dresselhaus 1955). Besides that, the occurrence of a multi-valley band means there is degeneracy. This is the sign of high electrical conductivity.

Besides thermoelectric material, Bi_2Se_3 is also a topological insulator. One of the main properties of the topological insulator is the presence of the magnetic field at the absence of applied magnetic field from the macroscopic scale. This effect is known as the quantum Hall effect which is Hall effect that occurs at quantum state with the absence of the magnetic field (Novoselov et al. 2007). This effect gives unique properties to Bi_2Se_3 such as time-reversal symmetry protection and protection from non-magnetic impurities. Any non-magnetic impurities that put on the material would not change its properties due to its topological nature (Xu et al. 2017). The role of SOC is the correction method to calculate an additional magnetic field that occurs in the material. SOC gives spin-dependent force to the moving electron that yields the occurrence of the magnetic field. However, SOC could not produce the quantum Hall effect because it breaks time-reversal symmetry. Despite that, SOC induce a quantum spin Hall effect that can conserve the symmetry due to the reliance on the spin of the electron. Thus, instead of time-reversal symmetry, SOC provides protection based on the spin conservation symmetry. This is the main reason for the necessity of SOC in the calculation for Bi_2Se_3. Without SOC, the band gap is inconsistent with the experimental works due to the absence of the main properties of Bi_2Se_3.

The effect of SOC is significant on the heavy element, which in this study, bismuth is one of the heavy elements. This is important for SOC to modify the electronic structure. In addition, a small band gap is another important factor for SOC to have a significant effect in the calculation (Parker & Singh 2011; Shi et al. 2015).

From the result of DOS without the inclusion of SOC as shown in Figure 3, it shows that Se-p has most population contribution at the valence band of electronic structure with the peak of 1.4 States/eV and energy range from 0 eV to -5.5 eV. Se-p partially hybridized with Bi-p and Bi-s. At the conduction band, Se-p has the most contribution with almost fully hybridized with Bi-p and density peak of 0.5 States/eV and energy range occupation from 0 eV to 5.0 eV.

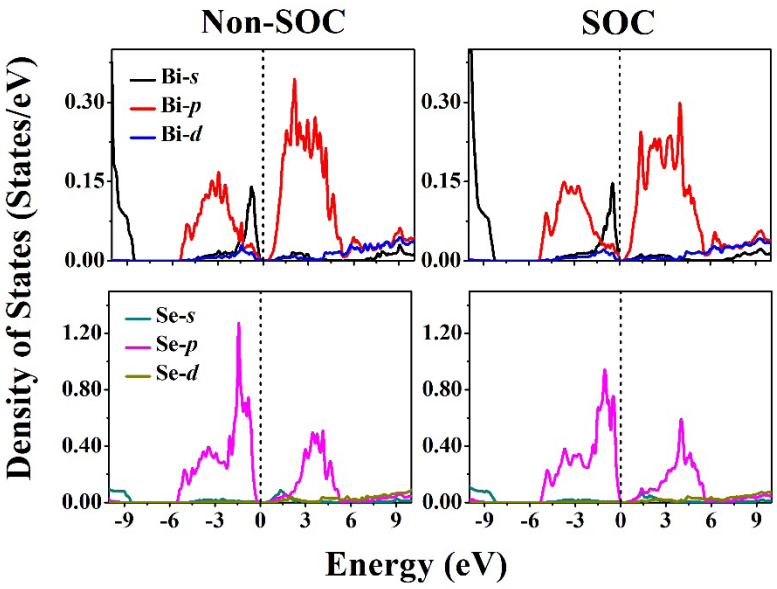

FIGURE 3. Density of states (DoS) of Bi_2Se_3 without SOC and inclusion of SOC

From the DOS with the inclusion of SOC, the pattern of population contribution is almost the same but the density peak of Se-p is reduced to 1.0 States/eV at the valence band. Se-p possesses the most contribution at the conduction band with strong hybridization with Bi-p. The hybridization of Se-p and Bi-4p occupied at energy range from 0 to 5.5 eV. The occupation of electrons without SOC is higher which indicates higher electrical conductivity.

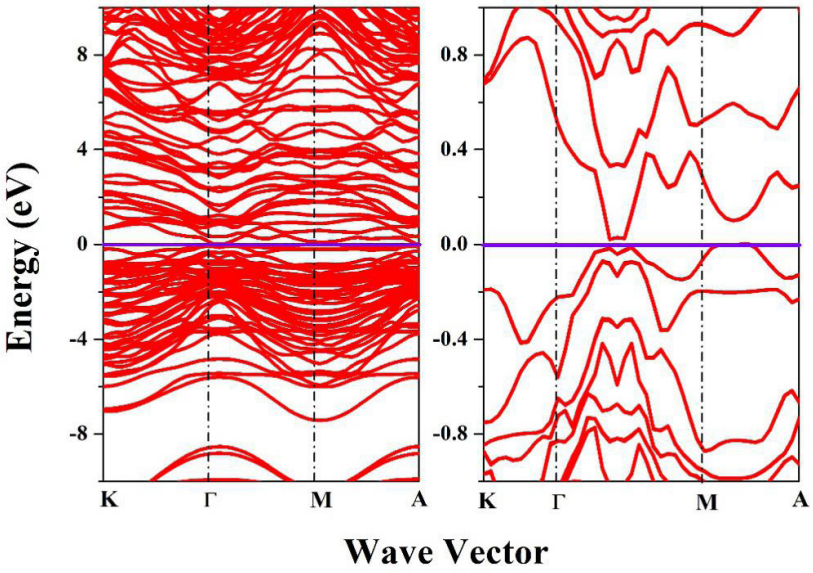

FIGURE 4. Band structure of Ni-doped Bi_2Se_3

Band structure of Ni-doped Bi_2Se_3 is calculated as shown in Figure 4 to analyse the changing of band structure when Bi_2Se_3 is doped with nickel. Ni-doped Bi_2Se_3 has an indirect band gap of 0.025 eV. The band gap is reduced considerably by 89.58% from 0.24 eV. This finding is supported by Feng et al. (2017) and Saaed et al. (2014a). The increased degeneracy of hole at valence band can be observed at the range of -0.1 to 0.0 eV. This high degeneracy is due to the high level of doping which shows that nickel gives a significant effect on the band structure of Bi_2Se_3. High level of doping and degeneracy has shifted the nature of semiconductors to act more like semi-metal. Near the Fermi level, the band valley at the valence band has decreased. However, the degeneracy is increasing. The increased degeneracy indicates the increase of electrons carriers thus increasing the thermopower of Bi_2Se_3. High degeneracy and reduced band gap show the sign of higher electrical conductivity. High degeneracy shows there are multiple indirect band gap occurred, thus thermal conductivity is increased.

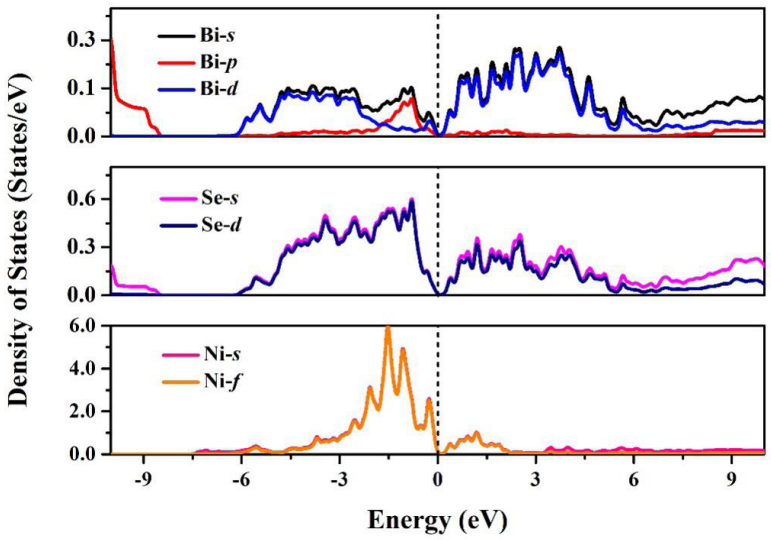

FIGURE 5. Density of states of Ni-doped Bi_2Se_3

The density of states of Ni-doped Bi_2Se_3 is calculated and the result is shown in Figure 5. Nickel gives considerable effect to the occupancy of holes at the valence band. Ni-*f*and Ni-*s* are most contributed at both valence and conduction band at the range of energy from 0 to -4 eV and 0 to 2 eV, respectively. Se-*s* and Se-*d* are strongly hybridized at valence and conduction band that indicates a strong covalent bond among Se atoms. The strong hybridization also occurred on Ni-*s* and Ni-*f*. The density of Ni-*s* and Ni-*f* reaches a peak of 6 states/eV. At the conduction band, the Ni-*s* and Ni-*f* density are far smaller than their respective density at the valence band. However, the occupation of electrons is higher than pure Bi_2Se_3. The density at the conduction band is increased by around 66.66% from ~0.6 to ~1.0. This shows the increase of electrical conductivity.

THERMOELECTRIC PROPERTIES

The thermoelectric properties of Bi_2Se_3 and Ni-doped Bi_2Se_3 are calculated and tabulated in Tables 5 and 6, respectively. The data from each table were used to plot a graph for each thermoelectric properties that consist of thermopower *S*, electrical conductivity σ, thermal conductivity κ and figure of merit *ZT* as shown in Figure 6. A comparison is made between Bi_2Se_3 and its Ni-doped based on each correspondence thermoelectric properties.

TABLE 5. Thermoelectric properties of Bi_2Se_3

T(K)	*S* ($\mu V/K$)	σ (S/cm)	κ (W/mk)	ZT
300	86.888	179.898	0.021	0.020
350	154.649	429.955	0.049	0.072
400	189.568	857.098	0.099	0.125
450	206.718	1501.186	0.173	0.167
500	214.300	2389.286	0.274	0.200

TABLE 6. Thermoelectric properties of Ni-doped Bi_2Se_3

T(K)	*S* ($\mu V/K$)	σ (S/cm)	κ (W/mk)	ZT
300	-64.733	84993.700	0.611	0.170
350	-69.413	85160.014	0.744	0.193
400	-73.481	85283.742	0.868	0.212
450	-76.911	85498.860	0.999	0.228
500	-79.727	85825.755	1.135	0.239

The thermopower of Bi_2Se_3 is increased from 300 to 500 K. Ni-doped Bi_2Se_3 also shows the same trend. However, doped by nickel has decreased the thermopower of Bi_2Se_3 over temperature. Positive values indicate that Bi_2Se_3 possesses a hole as a carrier, while Ni-doped Bi_2Se_3 has a negative value of thermopower which indicates electron as a carrier. Our thermoelectric results for pure Bi_2Se_3 is in good agreement with the experiments by percentage difference around 4 - 26% over temperature (Kadel et al. 2011; Sun et al. 2015a, 2015b, 2012). At 300 K, the thermopower has decreased by 25.49% which is undesirable. This is due to the decreased band gap. The decreased band gap would decrease the thermopower (Feng et al. 2017; Lee & Mahanti 2012). In addition, the thermopower of Ni-doped is steadily increased as the temperature increased by a change rate of approximately 3% - 6% for every 50 K. The change has decreased when compared with pure Bi_2Se_3 that has a change rate of around 3 - 78%.

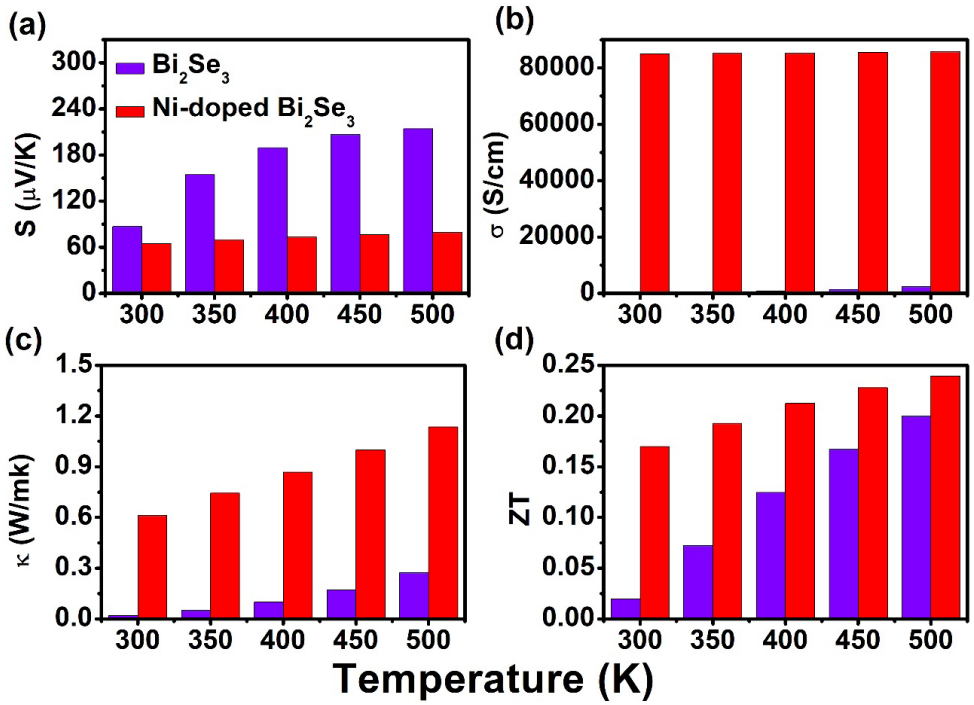

FIGURE 6. (a) Thermopower, (b) Electrical conductivity, (c) Thermal conductivity, and (d) Figure of merit of Bi_2Se_3 and Ni-doped Bi_2Se_3

The electrical conductivity can readily be derived from the transport distribution. Despite the disadvantage of the decreased band gap, it also gives advantages that contribute to the increased electrical conductivity. Decreased band gap would easily increase the electrons excitation from valence band to the conduction band, hence increase conductivity (Feng et al. 2017). Figure 5 shows electron occupancy is increased that indicates more electrons have excited and more electrical conductivity has occurred. Figure 6(b) shows increasing conductivity over temperature from 300 to 500 K for Bi_2Se_3 and its Ni-doped. Our results of electrical conductivity are in good agreement with the experiments by percentage difference around 1 - 15% over temperature (Kang et al. 2017; Saji et al. 2005; Sun et al. 2012a). Ni-doped has increased the electrical conductivity over temperature which is desirable for thermoelectric materials. Without Ni-doped, Bi_2Se_3 has an electrical conductivity change rate of around 66 - 82% from 300 to 400 K and decreased to 55% as the temperature reached 450 K. With Ni-doped, Bi_2Se_3 has a steady rate of change around 0.19 - 0.38%. Ni-doped has reduced the change rate of electrical conductivity of Bi_2Se_3 over temperature.

Thermal conductivity consists of two components which are electronic thermal conductivity and lattice thermal conductivity. In our study, we calculated only electronic thermal conductivity. Electronic thermal conductivity is strongly influenced by electrical conductivity through Wiedemann-Franz law. The law state that increased electrical conductivity would also increase thermal conductivity (Bejan & Kraus 2003). Our results of thermal conductivity for pure Bi_2Se_3 are in good agreement with the experiments by percentage difference around 14 - 23% at temperature 350 and 400 K and underestimate around 48 - 66% at temperature 300, 350, and 500 K (Adam et al. 2018; Kang et al. 2017; Sun et al. 2015a). Doped with nickel has increased the thermal conductivity over temperature due to the increased electrical conductivity.

Ni-doped has increased the thermal conductivity of Bi_2Se_3 from 0.021 to 0.611 W/mK at 300 K which is undesirable for thermoelectric material. However, the high electrical conductivity of Ni-doped Bi_2Se_3 has overcome the rising of thermal conductivity and thus improves the performance of Bi_2Se_3. Besides the influence from the electrical conductivity, the higher thermal conductivity also is due to the lattice contribution from indirect band gap at large maximum valence band to minimum conduction band at M to A. Without Ni-doped, the change rate of Bi_2Se_3 thermal conductivity is high up to 81% from 300 to 350 K. When the temperature increased to 400 K, the

thermal conductivity increased by 66%. The change rate decreasing down to 45% as the temperature reached 450 to 500 K. With Ni-doped, the change rate decreased around 13 - 20% over temperature from 300 to 500 K.

It can be observed in Figure 6(d) that the figure of merit (ZT) of Bi_2Se_3 is very low and not efficient to develop a thermoelectric device at room temperature. The results we obtained are in agreement with the experimental works by percentage difference around 2 - 36% (Kang et al. 2017; Kulsi et al. 2017; Min et al. 2015, 2013). Meanwhile, Ni-doped has improved the performance of Bi_2Se_3 by 750% for 300 K from 0.020 to 0.170. The ZT of Ni-doped Bi_2Se_3 increases steadily over temperature around with a change rate of around 5% - 12% for every 50 from 300 K.

Conclusion

The presence of nickel has changed the structure of Bi_2Se_3, forming a new bond and layer. The decreased bond length has increased electrical conductivity. The band gap of Bi_2Se_3 is in agreement with other available experimental studies with the inclusion of SOC. The SOC effect is necessary for the Bi_2Se_3 to show its band gap correctly due to its unique properties as a topological insulator. SOC effect give significant change such as multi-valley band, high degeneracy and multiple occurrences of indirect band gap. Bi_2Se_3 showed a poor thermoelectric material and thus, make it less efficient for application. However, Ni-doped has improved the performance of Bi_2Se_3 greatly and very suitable for room temperature thermoelectric devices. Ni has decreased the band gap Bi_2Se_3 and increase the occupation of electrons which indicates the increase in electrical conductivity and thermal conductivity. The decreased band gap has decreased thermopower. In addition, the occurrence of indirect band gap from a large maximum valence band to minimum conduction has also increased thermal conductivity. Despite the undesirable alteration of thermal conductivity and thermopower, the massive increase of electrical conductivity has overcome the deterioration.

Acknowledgements

This work was supported by the Ministry of Education (MOE) Malaysia under FRGS grant 600-IRMI/FRGS 5/3 (031/2017) and Universiti Teknologi MARA (UiTM) and Universiti Teknologi Malaysia (UTM) for the facilities provided.

References

Adam, A.M., Elshafaie, A., Mohamed, A.E.A., Petkov, P. & Ibrahim, E.M.M. 2018. Thermoelectric properties of Te doped bulk Bi_2Se_3 system. *Materials Research Express* 5(3): 035514.

Aguilera, I., Friedrich, C., Bihlmayer, G. & Blügel, S. 2013. GW study of topological insulators Bi_2Se_3, Bi_2Te_3, and Sb_2Te_3: Beyond the perturbative one-shot approach. *Physical Review B* 88(4): 045206-1-045206-7.

Ali, Z., Butt, S., Cao, C., Butt, F.K., Tahir, M., Tanveer, M., Aslam, I., Rizwan, M., Idrees, F. & Khalid, S. 2014. Thermochemically evolved nanoplatelets of bismuth selenide with enhanced thermoelectric figure of merit. *AIP Advances* 4(11): 117129-1-117129-8.

Augustine, S., Ravi, J., Ampili, S., Rasheed, T.M.A., Nair, K.P.R., Endo, T. & Mathai, E. 2003. Effect of Te doping and electron irradiation on thermal diffusivity of Bi_2Se_3 thin films by photo-thermal technique. *Journal of Physics D: Applied Physics* 36(8): 994-1000.

Bashir, M.B.A., Said, S.M., Sabri, M.F.M., Miyazaki, Y., Shnawah, D.A.A., Shimada, M. & Elsheikh, M.H. 2018. Enhancement of thermoelectric properties of $Yb_{0.25}Co_4Sb_{12}$ skutterudites through Ni substitution. *Sains Malaysiana* 47(1): 181-187.

Bejan, A. & Kraus, A.D. 2003. *Heat Transfer Handbook.* Vol. 1. New York: John Wiley & Sons.

Blaha, P., Schwarz, K., Madsen, G.K.H., Kvasnicka, D. & Luitz, J. 2001. Computer code WIEN2K. Austria: Vienna University of Technology.

Boledzyuk, V.B., Kovalyuk, Z.D., Kudrinskii, Z.R. & Shevchenko, A.D. 2015. Structural characteristics and magnetic properties of cobalt-intercalated A_2^5 B_3^6 single crystals. *Technical Physics* 60(11): 1658-1662.

Cermak, P., Ruleová, P., Holy, V., Prokleska, J., Kucek, V., Pálka, K., Benes, L. & Drasar, C. 2018. Thermoelectric and magnetic properties of Cr-doped single crystal Bi_2Se_3– search for energy filtering. *Journal of Solid State Chemistry* 258: 768-775.

Chang, C., Xiao, Y., Zhang, X., Pei, Y., Li, F., Ma, S., Yuan, B., Liu, Y., Gong, S. & Zhao, L.D. 2016. High performance thermoelectrics from earth-abundant materials: Enhanced figure of merit in PbS through nanostructuring grain size. *Journal of Alloys and Compounds* 664: 411-416.

Chis, V., Sklyadneva, I.Y., Kokh, K.A., Volodin, V.A., Tereshchenko, O.E. & Chulkov, E.V. 2012. Vibrations in binary and ternary topological insulators: first-principles calculations and raman spectroscopy measurements. *Physical Review B* 86(17): 174304.

Dresselhaus, G. 1955. Spin-orbit coupling effects in zinc blende structures. *Physical Review* 100(2): 580-586.

Dun, C., Hewitt, C.A., Huang, H., Xu, J., Montgomery, D.S., Nie, W., Jiang, Q. & Carroll, D.L. 2015. Layered Bi_2Se_3 nanoplate/polyvinylidene fluoride composite based n-type thermoelectric fabrics. *ACS Applied Materials & Interfaces* 7(13): 7054-7059.

Feng, B., Li, Q., Hou, Y., Zhang, C., Jiang, C., Hu, J., Xiang, Q., Li, Y., He, Z. & Fan, X. 2017. Enhanced thermoelectric properties of Sb-doped BiCuSeO due to decreased band gap. *Journal of Alloys and Compounds* 712: 386-393.

Hagmann, J.A., Li, X., Chowdhury, S., Dong, S.N., Rouvimov, S., Pookpanratana, S.J., Yu, K.M., Orlova, T.A., Bolin, T.B., Segre, C.U., Seiler, D.G., Richter, C.A., Liu, X., Dobrowolska, M. & Furdyna, J.K. 2017. Molecular beam epitaxy growth and structure of self-assembled Bi_2Se_3/Bi_2MnSe_4 multilayer heterostructures. *New Journal of Physics* 19(8): 085002.

Han, C., Li, Z. & Dou, S. 2014. Recent progress in thermoelectric materials. *Chinese Science Bulletin* 59(18): 2073-2091.

Hasan, S.W., Said, S.M., Abu Bakar, A.S., Jaffery, H.A. & Sabri, M.F.M. 2018. The role of electrolyte fluidity on the power generation characteristics of thermally driven electrochemical cells. *Sains Malaysiana* 47(2): 403-408.

Hor, Y.S., Richardella, A., Roushan, P., Xia, Y., Checkelsky, J.G., Yazdani, A., Hasan, M.Z., Ong, N.P. & Cava, R.J. 2009. p-type Bi_2Se_3 for topological insulator and low-temperature thermoelectric applications. *Physical Review B* 79(19): 195208.

Janíček, P., Drašar, C., Beneš, L. & Lošťák, P. 2009. Thermoelectric properties of Tl-doped Bi_2Se_3 single crystals. *Crystal Research and Technology* 44(5): 505-510.

Kadel, K., Kumari, L., Li, W.Z., Huang, J.Y. & Provencio, P.P. 2011. Synthesis and thermoelectric properties of Bi_2Se_3 nanostructures. *Nanoscale Research Letters* 6(1): 57.

Kang, Y., Zhang, Q., Fan, C., Hu, W., Chen, C., Zhang, L., Yu, F., Tian, Y. & Xu, B. 2017. High pressure synthesis and thermoelectric properties of polycrystalline Bi_2Se_3. *Journal of Alloys and Compounds* 700: 223-227.

Kulbachinskii, V.A., Kytin, V.G., Kudryashov, A.A & Tarasov, P.M. 2012. Thermoelectric properties of Bi_2Te_3, Sb_2Te_3 and Bi_2Se_3 single crystals with magnetic impurities. *Journal of Solid State Chemistry* 193: 47-52.

Kulsi, C., Kargupta, K. & Banerjee, D. 2017. Effect of nickel doping on thermoelectric properties of bismuth selenide. In *AIP Conference Proceedings*.

Lawal, A. & Shaari, A. 2017. Density functional theory study of electronic properties of Bi_2Se_3 and Bi_2Te_3. *Malaysian Journal of Fundamental and Applied Sciences* 12(3): 99-101.

Lee, M.S. & Mahanti, S.D. 2012. Validity of the rigid band approximation in the study of the thermopower of narrow band gap semiconductors. *Physical Review B* 85(16): 165149.

Lin, H., Das, T., Okada, Y., Boyer, M.C., Wise, W.D., Tomasik, M., Zhen, B., Hudson, E.W., Zhou, W., Madhavan, V., Ren, C.Y., Ikuta, H. & Bansil, A. 2013. Topological dangling bonds with large spin splitting and enhanced spin polarization on the surfaces of Bi_2Se_3. *Nano Letters* 13(5): 1915-1919.

Lind, H., Lidin, S. & Häussermann, U. 2005. Structure and bonding properties of $(Bi_2Se_3)_m(Bi_2)_n$ stacks by first-principles density functional theory. *Physical Review B* 72(18): 184101.

Madsen, G.K.H. & Singh, D.J. 2006. BoltzTraP. A code for calculating band-structure dependent quantities. *Computer Physics Communications* 175(1): 67-71.

Martinez, G., Piot, B.A., Hakl, M., Potemski, M., Hor, Y.S., Materna, A., Strzelecka, S.G., Hruban, A., Caha, O., Novak, J., Dubroka, A., Drasar, C. & Orlita, M. 2017. Determination of the energy band gap of Bi_2Se_3. *Scientific Reports* 7(1): 6891.

Min, Y., Park, G., Kim, B., Giri, A., Zeng, J., Roh, J.W., Kim, S.I., Lee, K.H. & Jeong, U. 2015. Synthesis of multishell nanoplates by consecutive epitaxial growth of Bi_2Se_3 and Bi_2Te_3 nanoplates and enhanced thermoelectric properties. *ACS Nano* 9(7): 6843-6853.

Min, Y., Roh, J.W., Yang, H., Park, M., Kim, S.I., Hwang, S., Lee, S.M., Lee, K.H. & Jeong, U. 2013. Surfactant-free scalable synthesis of Bi_2Te_3 and Bi_2Se_3 nanoflakes and enhanced thermoelectric properties of their nanocomposites. *Advanced Materials* 25(10): 1425-1429.

Mirhosseini, H. & Henk, J. 2012. Spin texture and circular dichroism in photoelectron spectroscopy from the topological insulator Bi_2Te_3: First-principles photoemission calculations. *Physical Review Letters* 109(3): 036803.

Mishra, S.K., Satpathy, S. & Jepsen, O. 1997. Electronic structure and thermoelectric properties of bismuth telluride and bismuth selenide. *Journal of Physics: Condensed Matter* 9(2): 461-470.

Nakajima, S. 1963. The crystal structure of Bi_2Te_3- xSex. *Journal of Physics and Chemistry of Solids* 24(3): 479-485.

Novoselov, K.S., Jiang, Z., Zhang, Y., Morozov, S.V., Stormer, H.L., Zeitler, U., Maan, J.C., Boebinger, G.S., Kim, P. & Geim, A.K. 2007. Room-temperature quantum Hall effect in graphene. *Science* 315(5817): 1379.

Park, K.H., Mohamed, M., Aksamija, Z. & Ravaioli, U. 2015. Phonon scattering due to van der Waals forces in the lattice thermal conductivity of Bi_2Te_3 thin films. *Journal of Applied Physics* 117(1): 015103.

Parker, D. & Singh, D.J. 2011. Potential thermoelectric performance from optimization of hole-doped Bi_2Se_3. *Physical Review X* 1(2): 021005.

Perdew, J.P. & Zunger, A. 1981. Self-interaction correction to density-functional approximations for many-electron systems. *Physical Review B* 23(10): 5048-5079.

Richards, W.G., Trivedi, H.P. & Cooper, D.L. 1981. *Spin-Orbit Coupling in Molecules*. Oxford: Oxford University Press.

Saeed, Y., Singh, N. & Schwingenschlögl, U. 2014a. Enhanced thermoelectric figure of merit in strained Tl-doped Bi_2Se_3. *Applied Physics Letters* 105(3): 031915-031915-4.

Saeed, Y., Singh, N. & Schwingenschlögl, U. 2014b. Thickness and strain effects on the thermoelectric transport in nanostructured Bi_2Se_3. *Applied Physics Letters* 104(3): 033105.

Saji, A., Ampili, S., Yang, S.H., Ku, K.J. & Elizabeth, M. 2005. Effects of doping, electron irradiation, H^+ and He^+ implantation on the thermoelectric properties of Bi_2Se_3 single crystals. *Journal of Physics: Condensed Matter* 17(19): 2873.

Shi, H., Parker, D., Du, M.H. & Singh, D.J. 2015. Connecting thermoelectric performance and topological-insulator behavior: Bi_2Te_3 and Bi_2Te_2 Se from first principles. *Physical Review Applied* 3(1): 014004.

Sun, G.L., Li, L.L., Qin, X.Y., Li, D., Zou, T.H., Xin, H.X., Ren, B.J., Zhang, J., Li, Y.Y. & Li, X.J. 2015a. Enhanced thermoelectric performance of nanostructured topological insulator Bi_2Se_3. *Applied Physics Letters* 106(5): 053102.

Sun, G., Qin, X., Li, D., Zhang, J., Ren, B., Zou, T., Xin, H., Paschen, S.B. & Yan, X. 2015b. Enhanced thermoelectric performance of n-type Bi2Se3 doped with Cu. *Journal of Alloys and Compounds* 639: 9-14.

Sun, Y., Cheng, H., Gao, S., Liu, Q., Sun, Z., Xiao, C., Wu, C., Wei, S. & Xie, Y. 2012. Atomically thick bismuth selenide freestanding single layers achieving enhanced thermoelectric energy harvesting. *Journal of the American Chemical Society* 134(50): 20294-20297.

Tan, G., Shi, F., Hao, S., Chi, H., Zhao, L.D., Uher, C., Wolverton, C., Dravid, V.P. & Kanatzidis, M.G. 2015. Codoping in SnTe: Enhancement of thermoelectric performance through

synergy of resonance levels and band convergence. *Journal of the American Chemical Society* 137(15): 5100-5112.
Tan, Q., Zhao, L.D., Li, J.F., Wu, C.F., Wei, T.R., Xing, Z.B. & Kanatzidis, M.G. 2014. Thermoelectrics with earth abundant elements: Low thermal conductivity and high thermopower in doped SnS. *Journal of Materials Chemistry A* 2(41): 17302-17306.
Urkude, R.R., Sagdeo, A., Rawat, R., Choudhary, R.J., Asokan, K., Ojha, S. & Palikundwar, U.A. 2018. Observation of Kondo behavior in the single crystals of Mn-doped Bi_2Se_3 topological insulator. *AIP Advances* 8(4): 045315.
Valla, T., Pan, Z.H., Gardner, D., Lee, Y.S. & Chu, S. 2012. Photoemission spectroscopy of magnetic and nonmagnetic impurities on the surface of the Bi_2Se_3 topological insulator. *Physical Review Letters* 108(11): 117601.
Wang, B.T., Souvatzis, P., Eriksson, O. & Zhang, P. 2015. Lattice dynamics and chemical bonding in Sb_2Te_3 from first-principles calculations. *The Journal of Chemical Physics* 142(17): 174702.
Wang, B.T. & Zhang, P. 2012. Phonon spectrum and bonding properties of Bi_2Se_3: Role of strong spin-orbit interaction. *Applied Physics Letters* 100(8): 082109.
Xu, N., Xu, Y. & Zhu, J. 2017. Topological insulators for thermoelectrics. *npj Quantum Materials* 2(1): 51.

Muhammad Zamir Mohyedin, Mohamad Fariz Mohamad Taib*, Masnawi Mustaffa & Oskar Hasdinor Hassan
Faculty of Applied Sciences
Universiti Teknologi MARA
40450 Shah Alam, Selangor Darul Ehsan
Malaysia

Muhammad Zamir Mohyedin & Mohamad Fariz Mohamad Taib*
Ionic, Materials and Devices (iMADE) Research Laboratory
Institute of Science
Universiti Teknologi MARA
40450 Shah Alam, Selangor Darul Ehsan
Malaysia

Afiq Radzwan & Amiruddin Shaari
Department of Physics, Faculty of Science
Universiti Teknologi Malaysia
81310 Skudai, Johor Darul Takzim
Malaysia

Bakhtiar Ul-Haq
Advanced Functional Materials & Optoelectronic Laboratory (AFMOL)
Faculty of Science
King Khalid University
9004 Abha
Saudi Arabia

Oskar Hasdinor Hassan
Faculty of Art & Design
Universiti Teknologi MARA
40450 Shah Alam, Selangor Darul Ehsan
Malaysia

Muhd Zu Azhan Yahya
Faculty of Defence Science & Technology
Universiti Pertahanan Nasional Malaysia
57100 Kuala Lumpur, Federal Territory
Malaysia

*Corresponding author; email: mfariz@uitm.edu.my

Received: 10 April 2020
Accepted: 20 May 2020